A LETTERS JOURNAL EXPLORING THE FRONTIERS OF PHYSICS

OFFPRINT

Exploring matter wave scattering by means of the phase diagram

JENG YI LEE and RAY-KUANG LEE

EPL, **124** (2018) 30006

epl

A Letters Journal Exploring the Frontiers of Physics

AN INVITATION TO SUBMIT YOUR WORK

epljournal.org

The Editorial Board invites you to submit your Letters to EPL

Choose EPL, and you'll be published alongside original, innovative Letters in all areas of physics. The broad scope of the journal means your work will be read by researchers in a variety of fields; from condensed matter, to statistical physics, plasma and fusion sciences, astrophysics, and more.

Not only that, but your work will be accessible immediately in over 3,300 institutions worldwide. And thanks to EPL's green open access policy you can make it available to everyone on your institutional repository after just 12 months.

Run by active scientists, for scientists

Your work will be read by a member of our active and international Editorial Board, led by Bart Van Tiggelen. Plus, any profits made by EPL go back into the societies that own it, meaning your work will support outreach, education, and innovation in physics worldwide.

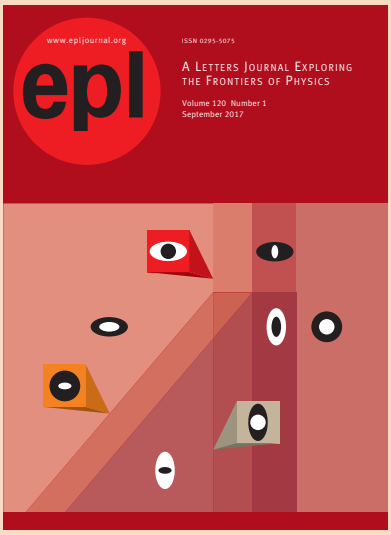

OVER

638,000

full-text downloads in 2017

Average submission to online publication

100 DAYS

21,500

citations in 2016

We greatly appreciate the efficient, professional and rapid processing of our paper by your team.

Cong Lin
Shanghai University

Four good reasons to publish with EPL

1. **International reach** – more than 3,300 institutions have access to EPL globally, enabling your work to be read by your peers in more than 90 countries.

2. **Exceptional peer review** – your paper will be handled by one of the 60+ co-editors, who are experts in their fields. They oversee the entire peer-review process, from selection of the referees to making all final acceptance decisions.

3. **Fast publication** – you will receive a quick and efficient service; the median time from submission to acceptance is 75 days, with an additional 20 days from acceptance to online publication.

4. **Green and gold open access** – your Letter in EPL will be published on a green open access basis. If you are required to publish using gold open access, we also offer this service for a one-off author payment. The Article Processing Charge (APC) is currently €1,400.

Details on preparing, submitting and tracking the progress of your manuscript from submission to acceptance are available on the EPL submission website, **epletters.net**.

If you would like further information about our author service or EPL in general, please visit **epljournal.org** or e-mail us at **info@epljournal.org**.

EPL is published in partnership with:

European Physical Society

Società Italiana di Fisica

EDP Sciences

IOP Publishing

A Letters Journal Exploring the Frontiers of Physics

November 2018

EPL, **124** (2018) 30006
doi: 10.1209/0295-5075/124/30006

www.epljournal.org

Exploring matter wave scattering by means of the phase diagram

Jeng Yi Lee[1,2] and Ray-Kuang Lee[2,3,4]

[1] *Department of Applied Science, National Taitung University - Taitung 95092, Taiwan*
[2] *Institute of Photonics Technologies, National Tsing Hua University - Hsinchu 30013, Taiwan*
[3] *Physics Division, National Center for Theoretical Sciences - Hsinchu 30013, Taiwan*
[4] *Department of Physics, National Tsing Hua University - Hsinchu 30013, Taiwan*

received 21 August 2018; accepted in final form 25 October 2018
published online 6 December 2018

PACS 05.60.Gg – Quantum transport
PACS 03.65.Nk – Scattering theory
PACS 03.75.-b – Matter waves

Abstract – For matter wave scattering from passive quantum obstacles, based on probability conservation we propose a phase diagram in terms of phase and modulus of scattering coefficients to explore all possible directional scattering probabilities. In the phase diagram, we can not only have the physical bounds on scattering coefficients for all channels, but also indicate the probability competitions among absorption, extinction, and scattering cross-sections. With the help of this phase diagram, we discuss different scenarios to steer scattering probability distribution, through the interference between *s*- and *p*-channels. In particular, we reveal the required conditions to implement a quantum scatterer, *i.e.*, a quantum dot in semiconductor matrix, with a minimum (or zero) value in the scattering probability toward any direction. Two sets of realizable semiconductor materials and geometry are proposed for the desired probability distribution. Our results provide a guideline in designing quantum scatterers with controlling and sensing matter waves.

Introduction. – A deep understanding of the wave scattering in passive obstacles plays a crucial role in nanophotonics, with a variety of practical applications from nanoantennas, metasurfaces, sensors, imaging systems, to light harvesting [1,2]. Exotic scattering phenomena at the subwavelength scale have been revealed such as coherent perfect absorbers, superscatterers, invisible cloaks, directional radiation scatterers, and superabsorbers [3–9]. To have a universal picture of all the allowable scattering coefficients, we apply the concept of energy conservation law to absorption cross-section, resulting in a phase diagram for electromagnetic waves [10]. Regardless of the details on the geometric configurations and material properties, physical boundary and limitation for zero backward/forward scatterings, known as Kerker effects, can be easily illustrated in the phase diagram [11].

Similarly to the classical counterpart, discussions on quantum particles encountering collisions have been an extensive research subject with different physical disciplines. For ultracold atoms of ^{87}Rb, the Fano-signature interference in quantum scattering, between resonant *d*-wave and the background *s*-wave, was observed experimentally [12,13]. Through the classical quantum correspondences between optical and matter waves, the concept for invisible cloaking has been applied to quantum scatterers formed by spherical quantum dots in core-shell heterostructures for a variety of applications, such as electron mobility control, enchancing thermoelectric power, and cloaking electronic devices [14–17]. Moreover, it was realized that even though the electron dynamics in graphene is governed by the relativistic massless Dirac equation, the approach to deal with the related scattering problem of electronic transport in graphene is similar to that used in the electromagnetic Mie theory [18–20]. Under the scattering picture, Klein tunneling, with a complete suppression in the backward direction, can be transformed as an isotropic scattering process with spin-orbital interactions [21].

To design quantum resonant scatterers at subwavelength scale, detailed physical quantities, such as effective mass, size, operating energy, and potential of a quantum particle, have been taken into account through higher-oder expansions [22]. Nevertheless, a systematic way to have all scattering solutions from quantum matter waves, irrespectively of the configuration in a scattering system, is still lacking. In this work, we consider the inelastic scattering from quantum matter waves, based on the Schrödinger equation. In terms of the phase and modulus of scattering

coefficients for passive quantum obstacles, we propose a phase digram to provide complete information among extinction, absorption and scattering cross-sections. With probability conservation, *i.e.*, the unitary relation, we discuss directional scatterings of matter waves by means of the phase diagram. Unlike the electromagnetic counterpart [6], a perfect zero scattering at specific angles can be achieved in quantum particles through the self-matter wave interference by s- and p-waves when they have the same phases and modulus. Moreover, a systematic way to realize scattering matter wave with a reduced scattering probability at any arbitrary direction is also demonstrated at the framework of the phase diagram. We also provide two sets of realizable semiconductor materials to support minimization scattering probabilities at forward or backward directions. Our results provide the guideline to design a directional quantum scatterer with matter waves.

Phase diagram for quantum scattering matter waves. – For a quantum particle with energy $E > 0$ and momentum along the z-direction, in the absence of a finite-ranged obstacle, the unbounded stationary eigenstates can be described by a plane wave, $\psi_i = e^{ikz}$, with the corresponding wave vector $\vec{k} = k\hat{z}$. Even though the introduction of a quantum obstacle may alter the original eigen-states, the corresponding eigen-energy remains unchanged in the elastic process. Then, one can apply the Lippmann-Schwinger equation to construct the new scattered state for a finite-ranged obstacle in an arbitrary shape [23].

Furthermore, if the scattering obstacle possesses rotational invariance, the Hamiltonian for the quantum matter wave commutes with angular momentum operators, *i.e.*, $\vec{L}^2$ and L_z, corresponding to the total and z-component angular-momentum operators, respectively. Further, we apply partial wave analysis to the matter wave scattering problem. In the asymptotic region, one can write down the wave function for the quantum obstacle as [24]

$$\psi(\vec{z}) = e^{i\vec{k}\cdot\vec{z}} + \frac{e^{ikr}}{r} f(\theta). \tag{1}$$

Here, we have the incident matter wave as a plane wave, and the corresponding scattering amplitude $f(\theta)$ can be defined as

$$f(\theta) = -\frac{i}{k}\sum_{l=0}^{l=\infty}(2l+1)a_l P_l(\cos\theta), \tag{2}$$

with the complex scattering coefficient a_l, the Legendre polynomial P_l, and the index in angular-momentum channels labeled as l. It is noted that a monopole ($l = 0$) is also called s-wave; while a dipole ($l = 1$) is called p-wave. From the asymptotic result shown in eq. (1), by integrating the probability flux along the radial component r over a closed area, we can directly find the corresponding absorption (also called as the reaction), scattering, and extinction cross-sections, respectively,

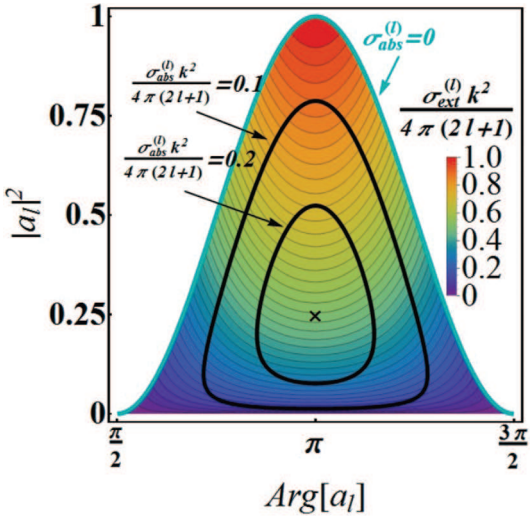

Fig. 1: (Color online) Phase diagram for quantum matter waves, defined by the phase $\mathrm{Arg}[a_l]$ and modulus $|a_l|^2$ of the scattering coefficient a_l, in each angular-momentum channel labeled by the index l. Here, the contour plot shows the value of the normalized extinction cross-section, defined as $\sigma_{ext}^{(l)} k^2 [4\pi(2l+1)]^{-1}$ with the range $[0, 1]$. Two different sets of constant normalized absorption cross-sections, defined as $\sigma_{abs}^{(l)} k^2 [4\pi(2l+1)]^{-1}$ bounded within $[0, 0.25]$, are depicted as black curves. The maximum value in the normalized absorption cross-section is also marked by the black cross, *i.e.*, $\sigma_{abs}^{(l)} k^2 [4\pi(2l+1)]^{-1} = 0.25$ located at $(\mathrm{Arg}[a_l], |a_l|^2) = (\pi, 0.25)$.

$$\sigma_{abs} = -\frac{4\pi}{k^2}\sum_{l=0}^{l=\infty}(2l+1)\{|a_l|^2 + Re[a_l]\}, \tag{3}$$

$$\sigma_{scat} = \frac{4\pi}{k^2}\sum_{l=0}^{l=\infty}(2l+1)|a_l|^2, \tag{4}$$

$$\sigma_{ext} = \sigma_{abs} + \sigma_{scat}. \tag{5}$$

One can see that in these convergent series, the dominant terms are often determined by environment size parameters, *i.e.*, ka with the effective range of the scatterer radius a [14,15,18]. We want to remark that through the optical theorem, the extinction cross-section is also linked to the scattering amplitude in the forward direction [23] $\sigma_{ext} = 4\pi\,\mathrm{Im}[f(0)]/k$. In addition, an alternative method to calculate the cross-section can use the phase shift δ_l, by re-defining the scattering coefficient as $2a_l + 1 = \exp[i\delta_l]$ [24].

With probability conservation, *i.e.*, the unitary relation, one can deduce that $\sigma_{abs}^{(l)} = 0$ (or $\sigma_{scat}^{(l)} = \sigma_{ext}^{(l)}$) for each angular-momentum channel. Here, $\sigma_{abs}^{(l)}$ is the partial absorption cross-section for the l-th channel, defined as $-4\pi(2l+1)\{|a_l|^2 + Re[a_l]\}/k^2$. Then, one can see that the unitary relation guarantees a real value for the phase shift, δ_l. On the contrary, if some incident quantum particles are annihilated by scattering obstacles or lose their

energy, we have $\sigma_{abs}^{(l)} > 0$ for a non-zero absorption cross-section. Next, we introduce a phasor representation for the scattering coefficients, by writing $a_l = |a_l| \exp\{i \operatorname{Arg}[a_l]\}$, into this inequality $\sigma_{abs}^{(l)} > 0$. As a result, a phase diagram for every partial extinction cross-section emerges naturally, as shown in fig. 1, defined by the phase $\operatorname{Arg}[a_l]$ and modulus $|a_l|^2$ of the scattering coefficient a_l, in each angular-momentum channel labeled by the index l. Here, we note that in this phase diagram, the vertical axis gives the strength in the scattering channel; while the horizontal axis reflects the phase in the scattering coefficient. Moreover, the colored region reveals all the allowable solutions for a passive quantum obstacle, *i.e.*, $\sigma_{abs}^{(l)} \geq 0$; while the uncolored (or in white color) regions correspond to unallowable solutions. Moreover, between the colored and uncolored regions, the boundary is depicted by a trajectory in light-blue color, which exactly follows the unitary relation.

In addition to the allowable solutions for scattering coefficients, in a single-phase diagram, one can also display information among the normalized absorption, scattering, and extinction cross-sections, defined as $\sigma_{abs}^{(l)} k^2/4\pi(2l+1)$, $\sigma_{scat}^{(l)} k^2/4\pi(2l+1)$, and $\sigma_{ext}^{(l)} k^2/4\pi(2l+1)$, respectively. As shown in fig. 1, the value of the normalized extinction cross-section is depicted in the contour plot, which is bounded within $[0, 1]$. Then, we also give two sets of constant absorption cross-sections in black color, $\sigma_{abs}^{(l)} k^2/4\pi(2l+1) = 0.1$ and 0.2, respectively. These black curves reveal non-trivial scattering events, with a constant absorption cross-section, but totally different extinction and scattering cross-sections. The maximum value in the normalized absorption cross-section is 0.25, see the black-cross marker, which reflects the resonance condition for a complete cancellation in the outgoing spherical matter wave, as $a_l = -0.5$ or $(\operatorname{Arg}[a_l], |a_l|^2) = (\pi, 0.25)$. Exotic scattering phenomena, such as quantum sensors [25] and anti-laser [26] can also be clearly illustrated in this phase diagram [10]. In addition, for the common adopted Born approximation to deal with weak scattering, valid for a shallow potential or a small particle size compared to the matter wave wavelength of quantum particles, the phase in the scattering coefficient is always $\pi/2$ or $3\pi/2$ (see footnote [1]). Moreover, for the case of annihilation of quantum particles, one can introduce a complex potential into the Schrödinger equation or impose an imaginary term on the phase shift [24,27] to model such a phenomenology, but this is beyond the scope of this work.

Interference from dominant *s*- and *p*-waves. – Although at a first glance, this phase diagram for quantum matter waves, shown in fig. 1, shares the same similarity to that introduced for the electromagnetic system, the underlined physical interpretations and properties are totally different. In quantum matter wave formalism, the physical measurement for probability is implemented through an ensemble average. Moreover, instead of electric and magnetic dipoles often excited in electromagnetic waves by subwavelength structures with proper materials [11], the two lowest orders for predominant scattering phenomena in a quantum subwavelength system are monopole and dipole, *i.e.*, *s*-wave with $l = 0$ and *p*-wave with $l = 1$, respectively.

Now, at the subwavelength scale, we study the differential scattering cross-section $\mathrm{d}\sigma_{scat}/\mathrm{d}\Omega$ for a quantum scatterer by calculating

$$\frac{\mathrm{d}\sigma_{scat}}{\mathrm{d}\Omega} = |f(\theta)|^2, \tag{6}$$

which means the ensemble average for probability scattered toward the angle θ [23].

In particular, we seek directional scattering events by asking for the zero probability distribution through the superposition from dominant *s*- and *p*-waves. This result means that there is a zero probability opportunity to detect such particles at this angle. This corresponds to find a family of solutions for the scattering coefficients a_0 and a_1 to satisfy the following condition:

$$a_0 + 3\, a_1 \cos\theta = 0, \tag{7}$$

or equivalently in the phasor representation:

$$|a_0| e^{i \operatorname{Arg}[a_0]} + 3|a_1| e^{i \operatorname{Arg}[a_1]} |\cos\theta| e^{i \operatorname{Arg}[\cos\theta]} = 0. \tag{8}$$

Here, θ is defined in the spherical coordinate, which is bounded by $[0, \pi]$. In the regime $\theta = [0, \pi/2]$, the argument of $\cos\theta$ would be 0; while when $\theta = [\pi/2, \pi]$, the argument is π.

Instead of trivial solutions, $a_0 = a_1 = 0$, let us consider the scenario when two scattering coefficients are the same both in their phase and modulus. Then, to satisfy the required condition given in eq. (7), we have $1 + 3\cos\theta = 0$, or equivalently $\theta = 109.5°$, which reveals a node (zero) in the corresponding probability distribution. It should be remarked that in this scenario, once the phase and modulus for *s*- and *p*-wave are the same, the system can possess any scattering cross-section, as indicated in fig. 1. We should stress that this finding, for the first time to our knowledge, is proposed clearly by our analysis and phase diagram.

For possible experimental implementation, we consider conducting electrons within a semiconductor matrix encountering an artificial quantum dot as an example. This artificial scatterer is constituted by two concentric spheres, with isotropic, homogeneous effective masses and potentials in the shell and core regions, denoted as (m_1, V_1) and (m_2, V_2) as illustrated in fig. 2(a), respectively. Effects of edge roughness and Coulomb screening are neglected for the illustration. With advances in fabrication technologies, quantum dots with a controllable size and tunable energy-band structure demonstrated recently can be

[1] In the first-order Born approximation, the corresponding scattering amplitude for a general potential is always a real number, but its sign (negative or positive) depends on the barrier or well in potentials [24], resulting in the phase of scattering coefficients being $\pi/2$ or $3\pi/2$.

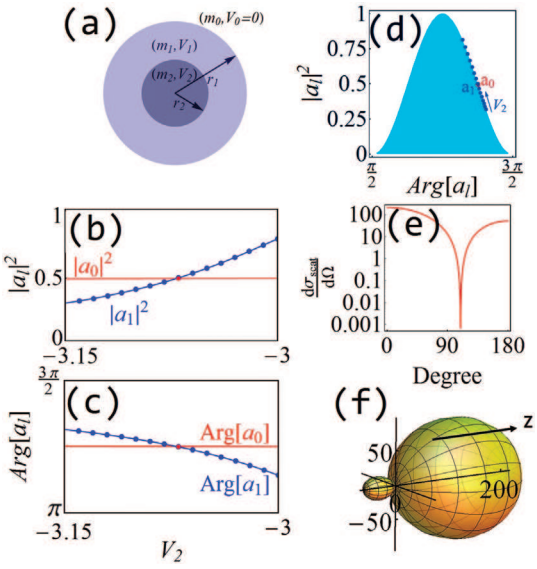

Fig. 2: (Color online) (a) Illustration of our quantum scatterer, formed by a two-layered quantum dot in the shape of a core-shell sphere. The corresponding (b) modulus and (c) phase for the the scattering coefficients: a_0 (s-wave) and a_1 (p-wave), in red and blue colors, respectively, as a function of the effective potential in the core region, V_2. Note that both in (b) and (c), two curves intersect at the same point with $V_2 = -3.07\,\text{eV}$. (d) The trajectories in the phase diagram for the solutions shown in (b) and (c). The differential scattering cross-sections as a function of the angles are shown in (e) log-plot and (f) 3D plot, with a clear dip (node) at $\theta = 109.5°$.

a good candidate as our quantum scatterer [28]. Here, we choose the system parameters from a single quantum dot as $r_1 = 4\,\text{nm}$ for the radius of the whole sphere, $r_2 = 0.4r_1$ for the core region, $E = 0.022\,\text{eV}$ for the incident energy, and $V_1 = -2.83\,\text{eV}$ for the effective potential in the shell region. As for the effective mass outside the quantum scatterer, inside the shell region, and inside the core region, we set $m_0 = 0.065\ m_e$, $m_1 = 0.034\ m_e$, and $m_2 = 0.021\ m_e$ (in the unit of electron mass m_e), respectively. Then, by scanning the effective potential in the core region, V_2, we report the changes in the modulus and phase for the corresponding scattering coefficients in the two lowest orders, a_0 and a_1, as shown in the red- and blue-colored curves of fig. 2(b) and (c), respectively. As one can see, in the range $V_2 = [-3.15\,\text{eV}, -3\,\text{eV}]$, there exists a crossing point from two scattering coefficients, which is located at the same effective potential in the core region, *i.e.*, $V_2 = -3.07\,\text{eV}$. At this effective potential, we have exactly $a_0 = a_1$, which gives the operation point to satisfy a directional scattering with a node at $\theta = 109.5°$.

For a lossless system, our Hamiltonian ensures a unitary relation, guaranteeing the scattering coefficients a_0 and a_1 located in the light-blue–colored trajectory shown in fig. 1. Regardless of the material parameters and geometry size, we have $\sigma_{abs}^{(l)} = 0$ due to the unitary relation. To illustrate such a trajectory along the boundary between allowable and unallowable regions, in fig. 2(d), we depict the locations from the solutions shown in figs. 2(b), (c) in the phase diagram. As one can see that, in this chosen range, $V_2 = [-3.15\,\text{eV}, -3\,\text{eV}]$, the corresponding modulus of scattering parameter for the p-wave, $|a_1|$, increases as V_2 increases; while the modulus for the s-wave, a_0, remains almost unchanged[2].

The advantage of the phase diagram includes not only the integrated information of phase and modulus for each scattering channel, but also the corresponding cross-sections at the same map. For the crossing point at $V_2 = -3.07\,\text{eV}$, we also calculate the corresponding differential scattering cross-section as a function of angles, as shown in fig. 2(e) and (f) for the log-plot and 3D plot, respectively.

Now, we go one step further by considering the case $a_0 \neq a_1$ in two scattering channels. For $\theta \in [0, \pi/2]$, the argument of $\cos\theta$ is 0. Thus, in order to minimize eq. (8), the arguments between a_0 and a_1 need to be out of phase, to form a destructive interference. As clearly illustrated in the phase diagram, such an out-of-phase condition can only be satisfied when this scattering obstacle is asked to support scattering events located in the two opposite boundaries. The corresponding condition for the modulus to satisfy eq. (8) becomes

$$\frac{|a_0|}{|a_1|} = 3|\cos\theta|. \tag{9}$$

As an example, in the first column of fig. 3, we demonstrate the scattering pattern with a minimization in the scattering distribution at $\theta = 72°$. The corresponding locations of the s- and p-wave channels in the phase diagram are depicted in fig. 3(a), while the resulting scattering distributions are represented in the log-plot and 3D plot, *i.e.*, fig. 3(b) and (c), respectively. Since the phase difference between a_0 and a_1 is almost π, one can expect to have a node in the scattering cross-section for $\theta \in [0, \pi/2]$. In this example, the system parameters used are all the same as those shown in fig. 2(f), but with $V_1 = 1.2\,\text{eV}$ and $V_2 = -2.4906\,\text{eV}$.

For $\theta \in [\pi/2, \pi]$, the argument of $\cos\theta$ is π. As a result, eq. (8) can be reduced to the condition $|a_0|e^{i\text{Arg}[a_0]} = 3|a_1|e^{i\text{Arg}[a_1]}|\cos\theta|$. Then, only when $\theta \in [\pi/2, \pi]$, we can have a minimum (or zero) value in the corresponding scattering distribution. Moreover, from the phase diagram shown in fig. 3(d), we can see that both a_0 and a_1 locate at the same side, minimizing their phase difference. Due to the same sign in the phases of a_0 and a_1, the resulting scattering pattern is enhanced along the forward direction. In figs. 3(e), (f), we report the differential scattering cross-section with a dip (node) at $\theta = 120°$. Here, the parameters are all the same as those in fig. 2(f), but with $V_1 = 1.2\,\text{eV}$ and $V_2 = -2.4884\,\text{eV}$.

It is known that for electromagnetic waves, Kerker *et al.* proposed to generate zero backward scattering

[2]It should be noted that in this case, by tuning V_2 p-wave can be excited to be on resonance to the background s-wave, forming a Fano signature in the scattering cross-section.

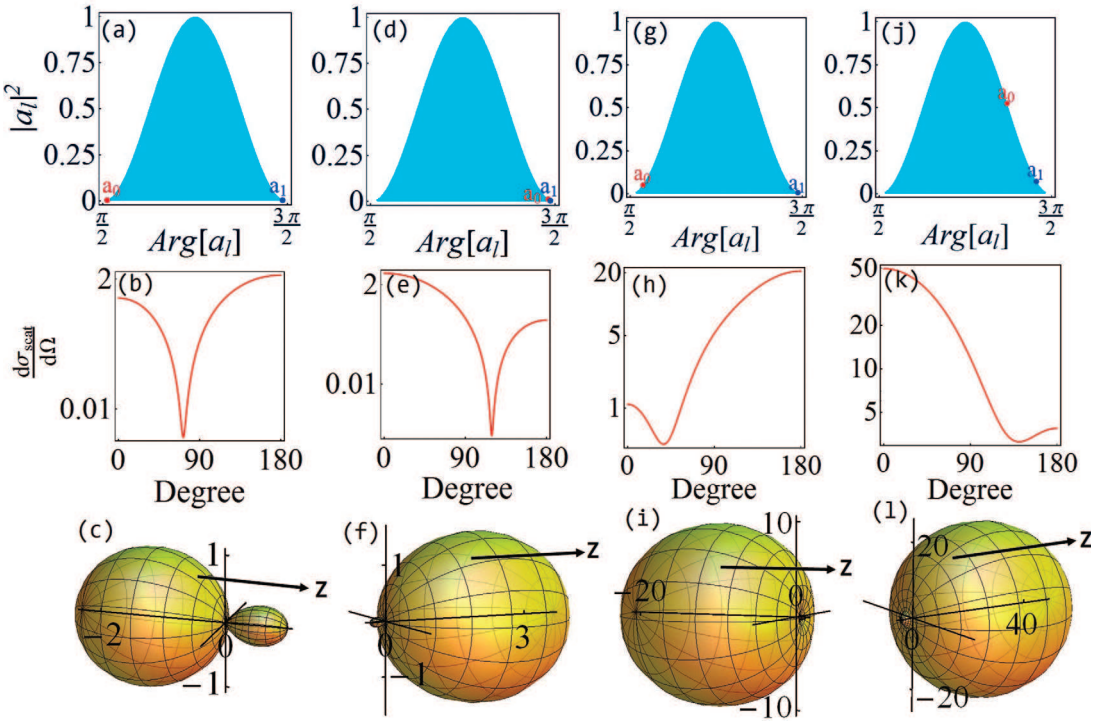

Fig. 3: (Color online) Four selective-angles to minimize the directional scattering cross-section. The corresponding locations of s and p in the phase diagram are shown in the first row ((a), (d), (g), (j)) corresponding to a minimum (or zero) value in the scatting angle at $\theta = 72°$, $120°$, $0°$ (nearly), and $180°$ (nearly). The resulting differential scattering cross-sections as a function of the angle are depicted in the second and third rows, for the log-plots and 3D plots, respectively.

(ZBS) and zero forward scattering (ZFS) through a proper combination of magnetic and electric dipoles [6]. However, due to the optical theorem, there is always a residue in the forward scattering direction for any passive electromagnetic scatterer. In our system, eliminating the scattered probability in the forward direction $\theta = 0$, the corresponding scattering amplitude $f(\theta = 0)$, shown in eq. (6), is also linked to the extinction cross-section. Instead of a perfect ZFS, we can only minimize the scatting distribution at the angle $\theta = 0$. To do this, by fixing $\theta = 0$, one can perform the minimization for $f(0)$ with the conditions $|a_0| = 3|a_1|$ and $\mathrm{Arg}[a_0] - \mathrm{Arg}[a_1] = \pm\pi$, meaning that the system would intrinsically have weak interaction with impinging matter wave.

Now, we consider a realizable semiconductor dot system constructed by AlSB(environment)/GaSb(shell)/AlSB(core) with a straddling alignment of the energy band structures. Within the Γ valley, the effective mass of the conduction electrons would be $m_0 = 0.14\ m_e$, $m_1 = 0.04\ m_e$ and $m_2 = 0.14\ m_e$ in which the conduction band offset of GaSb to AlSb is about $-0.5\,\mathrm{eV}$, representing a well potential [29]. As shown in the third column in fig. 3(g)–(i), we report the scattering pattern for matter waves with a nearly zero value in the forward scatting by using the parameters $r_1 = 6.89\,\mathrm{nm}$, $r_2 = 2\,\mathrm{nm}$, $E = 0.003\,\mathrm{eV}$ and $V_1 = -0.503\,\mathrm{eV}$. Furthermore, ZBS can be easily generated with a family of scattering events in the phase diagram [11]. A typical example for ZBS is illustrated in fig. 3(j), (k) with $r_1 = 3.5\,\mathrm{nm}$, $r_2 = 1.7\,\mathrm{nm}$, $E = 0.012\,\mathrm{eV}$ and $V_1 = -0.512\,\mathrm{eV}$.

We want to stress that although our discussion is limited to the plane-wave formalism of quantum scatterers, the partial wave decomposition is independent of the incident wave form. As for other geometry for the quantum scatterer, one may also find a suitable orthogonal basis to decompose the incident and scattered waves. All the physical principles we apply here consist in embedding the law of probability conservation on the absorption cross-section.

Before conclusion, we should note that in electromagnetism the polarization is a characteristic, but there is no equivalent correspondence in our studies. For the work by Kerker *et al.* [6], they found that only two directions can achieve zero field intensity, but in our case, with proper phase and amplitude, we can have a minimization probability distribution in the wanted direction. The finding of $\theta = 109.5°$, meeting a perfect zero of the scattering probability by the dominant s- and p- channels, is unique, which cannot be found in electromagnetism. In addition, extra divergence free constraints for electric and magnetic fields need to be carefully considered in electromagnetic vector solutions, but there is no such issue in our studies. Last but not least, it is well known that if one can control quantum particle mobility by a proper design of the obstacle (or defect), the property of the whole system would be dramatically changed. Such results have been practically

discussed in thermoelectric and graphene systems [17,18]. Our proposed architecture wants to highlight a conserved probability condition that is often neglected in scattering phenomena. As a result, the finding of a phase diagram and the consequences of its use can provide a framework to manipulate scattering probability, beyond any specific cases.

Conclusion. – In conclusion, by considering inelastic scattering for quantum matter waves with the condition $\sigma_{abs}^{(l)} > 0$, we propose a phase diagram for every angular-momentum channel. In the phase diagram, we can reveal not only the physical bounds on phase and modulus of scattering coefficients, but also indicate the competitions among absorption, extinction and scattering cross-sections. With the help of this phase diagram, we discuss different scenarios through the interference between s- and p-waves, with the demonstrations to steer the scattering probability distribution from quantum matter waves. We find that with the same phase and modulus from dominant channels, one can have a zero value in the scattering probability distribution at $\theta = 109.5°$. However, as the scattering coefficients in the s- and p-waves are different, we can also minimize the scatting probability distribution at a given angle, with proper phase and modulus. With an artificial core-shell quantum dot in the semiconductor matrix as an example, such a systematic way by means of the phase diagram is able to provide guidelines in the designing quantum scatterers. We also demonstrate how to realize systems in real semiconductor cases with zero scattering probability in the desirable directions. We believe that our discussion can be extended to recent hot topics such as controlling Dirac-electron motion in graphene 2D materials.

* * *

This work has been supported by the Ministry of Science and Technology, Taiwan, under Contract MOST 105-2686-M-007-003-MY4.

REFERENCES

[1] Kuznetsov A. I., Miroshnichenko A. E., Brongersma M. L., Kivshar Y. S. and Luk'yanchuk B., *Science*, **354** (2016) 2472.
[2] Novotny L. and Hulst N. V., *Nat. Photon.*, **5** (2011) 83.
[3] Noh H., Chong Y. D., Stone A. D. and Cao H., *Phys. Rev. Lett.*, **108** (2012) 186805.
[4] Ruan Z. and Fan S., *Phys. Rev. Lett.*, **105** (2010) 013901.
[5] Alú A. and Engheta N., *Phys. Rev. E*, **72** (2005) 016623.
[6] Kerker M., Wang D.-S. and Giles C. L., *J. Opt. Soc. Am.*, **73** (1983) 765.
[7] Fu Y. H., Kuznetsov A. I., Miroshnichenko A. E., Yu Y. F. and Lukyanchuk B., *Nat. Commun.*, **4** (2013) 1527.
[8] Person S., Jain M., Lapin Z., Saenz J. J., Wicks G. and Novotny L., *Nano Lett.*, **13** (2013) 1806.
[9] Estakhri N. M. and Alú A., *Phys. Rev. B*, **89** (2014) 121416(R).
[10] Lee J. Y. and Lee R.-K., *Opt. Express*, **24** (2016) 6480.
[11] Lee J. Y., Miroshnichenko A. E. and Lee R.-K., *Phys. Rev. A*, **96** (2017) 043846.
[12] Thomas N. R., Krgaard N., Julienne P. S. and Wilson A. C., *Phys. Rev. Lett.*, **93** (2004) 173201.
[13] Krgaard N., Mellish A. S. and Wilson A. C., *New J. Phys.*, **6** (2004) 146.
[14] Liao B. L., Zebarjadi M., Esfarjani K. and Chen G., *Phys. Rev. Lett.*, **109** (2012) 126806.
[15] Fleury R. and Alú A., *Phys. Rev. B*, **87** (2013) 045423.
[16] Lee J. Y. and Lee R.-K., *Phys. Rev. B*, **89** (2014) 155425.
[17] Zebarjadi M., Liao B., Esfarjani K., Dresselhaus M. and Chen G., *Adv. Mater.*, **25** (2013) 1577.
[18] Liao B., Zebarjadi M., Esfarjani K. and Chen G., *Phys. Rev. B*, **88** (2013) 155432.
[19] Heinisch R. L., Bronold F. X. and Fehske H., *Phys. Rev. B*, **87** (2013) 155409.
[20] Novikov D. S., *Phys. Rev. B*, **76** (2007) 245435.
[21] Asmar M. M. and Ulloa S. E., *Phys. Rev. Lett.*, **112** (2014) 136602.
[22] Lee J. Y., Miroshnichenko A. E. and Lee R.-K., *Phys. Lett. A*, **381** (2017) 2860.
[23] Sakurai J. J., *Modern Quantum Mechanics* (Addison-Wesley) 1994.
[24] Schwabl F., *Quantum Mechanics* (Springer) 2002.
[25] Fleury R. and Alú A., *Phys. Rev. B*, **87** (2013) 201106(R).
[26] Chong Y. D., Ge L., Cao H. and Stone A. D., *Phys. Rev. Lett.*, **105** (2010) 053901.
[27] Valentin L., *Subatomic Physics: Nuclei and Particles* (Hermann, Paris) 1981.
[28] Kagan C. R., Lifshitz E., Sargent E. H. and Talapin D. V., *Science*, **353** (2016) 6302.
[29] Adachi S., *Properties of Group-IV, III–V, and II–VI Semiconductors* (John Wiley & Sons Ltd., England) 2005.